ALMA memo 428. June 2002

Compact Configuration Evaluation

Melvyn Wright

Radio Astronomy laboratory, University of California, Berkeley, CA, 94720

ABSTRACT

In this memo, we compare the imaging performance of 3 compact configurations. We have written MIRIAD scripts to simulate imaging with ALMA, and pipeline the results into tables. We present a table of beam FWHM, brightness sensitivity and sidelobe levels as a function of declination. Single field images for source diameters 8, 16, 24, and 32 arcsec are also analyzed. Based on these results, 2 compact arrays appear sufficient. Omitting an extended N-S compact configuration is operationally simpler and saves $\sim$ \$1M.

1. Introduction

Three compact antenna configurations are being considered for ALMA:

Config 1 - A most compact array for maximum brightness sensitivity. At high declinations this array has shadowed antennas and an elongated beam.

Config 2 - A more Gaussian array with 1.5 times the resolution of config 1, this requires an extra 20 stations.

Config 3 - A N-S extended array with a circular beam and the same resolution as config 1 for declination 30 deg sources. Athough this uses many stations from the other configurations it is expensive, requiring an extra $\sim$ 25 stations to be built.

Apart from the cost ($\sim$ \$40,000 per station), multiple compact configurations require additional scheduling and antenna moves. There are now preliminary designs (J.Conway private communication, May 6, Figures 5–7), and a decision on the compact configurations needs to be made soon so that detailed engineering evaluation at the ALMA site can begin. The 3 configurations have already been designed to provide good uv-coverage. In this memo we evaluate the performance of each configuration for single field imaging. We characterize the configurations in terms of beam FWHM, sidelobe level and brightness sensitivity.

We also made single field imaging simulations for source diameters 8, 16, 24, and 32 arcsec at 230 GHz where the primary beam FWHM $\sim 24''$. These results are characterized by the total recovered

flux density and the image fidelity. The purpose of this memo is to compare the performance of the 3 configurations, not to perfect the deconvolution.

The most serious defect is the lack of baselines shorter than the 12m antenna diameter. Using single dish data and mosaicing will be discussed in a subsequent memo. Similar imaging simulations have been previously discussed in detail for observations with the CARMA array in bima memo 73, and the case for adding smaller antennas to the ALMA array in ALMA memo 272

2. The fitting procedures

The fitting procedures are simple **unix csh** scripts which control **MIRIAD** tasks. The results from two scripts are presented here. The first script generates uv-data for a point source with thermal and atmospheric phase noise, does a phase calibration, and makes an image and beam. A Gaussian fit is made to the synthesised beam, and the results written into a table. The brightness sensitivity, beam FWHM, and residual sidelobe level after the fit is listed in Table 1. Timing information for each step is given. The script takes $\sim$ 30s run time for each instance on a Sparc 10 workstation and the procedure could and probably should be part of the observing preparation tools.

The second script makes model uv-data using a VLA image of Cas A as a model. The model is scaled to various source sizes. Thermal noise, appropriate for ALMA is added to the uv-data. The uv-data is Fourier transformed to make images and deconvolved using both CLEAN and Maximum Entropy algorithms. The original image model is convolved to the same resolution by a Gaussian restoring beam and subtracted from the deconvolved image. The residual imaging errors are characterized in Table 2 by the total recovered flux, peak flux density and the RMS residuals. The script gives the time for each step, and takes $\sim$ 130s with a Maximum Entropy deconvolution. It seems quite reasonable that this procedure should also be part of the observation preparation tools, so that the proposer can see what is the likely outcome of the observations for a given source model.

3. Discussion

3.1. Beam FWHM, Sensitivity, Sidelobes levels, and Shadowing

Table 1a lists the beam FWHM, sensitivity, sidelobes levels, and fraction of the data remaining after shadowed data are omitted, for each configuration and source declinations from +60 to –60 deg. Each configuration was sampled from HA –1 to +1 hours at intervals of 1 minute. (2 hours is sufficient to give a well sampled uv-coverage. The Nyquist sample interval $\sim$ 4-10 min for the maximum baselines in these configurations.) We used natural weighting of the uv-data with a system temperature 40 K and a bandwidth 8 GHz.

Configuration 1 gives the largest beam FWHM and the best brightness sensitivity. This configura-

tion is severely shadowed at high declination as evidenced by the small percentage of un-shadowed visibility samples (Nvis), the high RMS and high sidelobes. The Gaussian configuration 2 gives almost as good brightness sensitivity as the stretched configuration 3, and has lower sidelobes in most cases. The benefits of configuration 3 seem marginal given the cost of the additional stations and the extra antenna moves required.

3.2. Shadowing

When an antenna is shadowed, all antenna pairs which include the shadowed antenna are omitted. Although the shortest baselines are excluded, this can also result in a larger beam FWHM when antennas on long baselines are shadowed. The efficiency of the configuration can be improved by including partially shadowed baselines. In Table 1b we list the results including data with up to 50% of the antenna shadowed. The sensitivity and sidelobe levels are both improved. Several possible effects of shadowing should be considered. i) a modified illumination pattern, ii) possible cross-talk between the shadowed antennas, iii) changes in the effective phase center of the antenna. We briefly discuss each of these.

i) A modified illumination pattern illumination pattern, gives a time and baseline dependent primary beam pattern. The change in the forward gain for a compact source is easily calculated, but the effective primary beam illumination for extended sources is more troublesome. For mosaic observations we would need to calculate a primary beam for each pointing, baseline, and integration. Whilst this is possible in principal, the increased computing burden is substantial, and the errors in the visibility data from pointing errors and uncertainties in the primary beam are large.

ii) Cross-talk between the shadowed antennas is not well understood. Sensitive experiments with closely spaced, and possibly shadowed antennas often corrupt the visibility data (e.g. Subrahmanyan 2002; Padin etal. 2001). Such cross-talk is not often seen at the BIMA array, where data are recorded for projected antenna spacings as short at half the antenna diameter. These data are flagged but can be used at the discretion of the user. Apart from the loss in amplitude, no cross-talk is seen down to low levels. The reason for these differences are not clear.

iii) When an antenna is partially shadowed the projected spacing (u,v) is changed. In principal, this can be computed and recorded with the uv-data. If there are several closely packed antennas, this could be quite complicated, as different parts of the antenna structures shadow neighboring antenna surfaces. The phase center, defined by the intersection of the antenna axes is unchanged (at least to 1st order, ignoring the variations in the effective elevation axis for different parts of the antenna surface).

In view of these difficulties it seems better not to rely on the shadowed data, despite the appeal of shorter projected spacings and increased observing efficiency. One further effect which should be considered is the possibility of deleterious effects at zero fringe rate, when any cross talk is not distinguished from the source correlation. The fringe rate is HDOT u cos(declination) Hz, where

HDOT = $7.25^{-5}s^{-1}$ and u is in wavelengths. Flagging these data over a Nyquist sample interval $\sim$ 5 min would leave a $\sim$ 46/cos(declination) λ gap at $u = 0$. This is not a major gap in the uv-coverage for ALMA.

4. Imaging

In this memo we will discuss only the results for single field imaging. Mosaic observations will be discussed in a separate memo. We made images for a range of source sizes from 8″ to 32″ at 230 GHz and investigated the ability of the 3 compact configurations to image these structures. At 230 GHz, the primary beam $\sim$ 24″ and $\lambda/D = 22.4''$ where D is the antenna diameter (and the shortest baseline without shadowing). We made images for source declinations +30 and –30 deg, and each configurations was only sampled from HA –1 to +1 hours in order to reduce the parameter space.

4.1. The Source Model

We used a scaled Cas A image as the source model. The actual source model used does not matter too much. We require a model which has structure over a wider range of spatial frequencies than those sampled by the different configurations, so we can see how well each configuration reproduces the sampled spatial frequencies, and those extrapolated to both larger and smaller scales. For the compact configurations we are particularly interested in the extrapolation to larger angular scales. Figure 1 shows radial distributions of the Fourier transform for the Cas A and eyechart model used in BIMA memo 73. The overall slope is quite close to a uniform disk model. At the highest spatial frequencies Cas A is deficient in small scale structure (Arendt & Dickel 1987). The eyechart model is somewhat flatter. When we compare deconvolved images with the model, the details and defects of the deconvolution algorithms enter into the comparison. Since these algorithms have been developed for astronomical source distributions, Cas A seems like a more appropriate source model to use. Comparison by eye is harder than with the eyechart, but the defects in the images are quite apparent when we subtract the original source model from the synthesised images.

4.2. Deconvolved Images

In Table 2 we characterize the image fidelity by the total flux, peak flux density, and residuals in the difference between the synthesised image and the original model convolved to the same resolution. The images were deconvolved using CLEAN and Maximum Entropy (MEM) algorithms. The total flux density in the model image is 732 Jy. The thermal noise is 2 μJy.

For the 8″ model, CLEAN recovers most of the total flux, and reproduces the source structure with an RMS residual of about 0.3% of the peak flux density (Table 2a). For the 16″ model, CLEAN is hard pressed to recover the large scale structure and total flux, but is helped by supplying a-priori

information such as a bounding region for the source. A multi-resolution CLEAN should be better, but this was not tried. MEM worked well provided the total flux was given as a-priori information; the RMS residual $\sim 0.1\%$ of the peak flux density. (Table 2b).

For the $24''$ and $32''$ models, the total flux density is no longer sufficient information to fill in for the missing interferometer spacings. The shortest spacing with no shadowing is 9200λ. The total flux and the image fidelity depend on the detailed sampling of the large scale structure and consequently vary with the source declination and configuration. For $24''$ (Table 2b), the RMS residual $\sim 0.5\%$ for declination –30, and $\sim 0.2\%$ for declination +30. For $32''$, the RMS residual $\sim 3\%$ at declination –30, and $\sim 0.2\%$ for declination +30. The improved performance at declination +30 is because shorter projected spacings are sampled. Shorter projected spacings can be sampled at declination –30 by observing away from transit, at the cost of increased atmospheric opacity and system noise at the higher frequencies. Figure 2 shows the MEM image and Cas A model for a $32''$ source size. Figure 3 shows the the difference between the MEM and the model convolved to the same resolution. The characteristic bowl due to the missing short spacings is the most serious defect. Using a single dish image and mosaicing will be discussed in a subsequent memo.

From these statistics, there is not much difference between the 3 sampled configurations. Configuration 1 give somewhat better image fidelity, but over a smaller range of spatial frequencies. The image fidelity is limited by uv-sampling rather than brightness sensitivity; configuration 2 serves just as well as configuration 3 at high declinations and is somewhat more versatile.

4.3. Comparisons in the Fourier domain

Since defects in images depend on the uv-sampling, it may be better to compare the model and the image in the Fourier domain – to evaluate the efficacy of the configurations in sampling the source structure on different scales. We made Fourier transforms of the models and deconvolved images. The obvious defects are in the unsampled short uv-spacings. Adding the total flux does not fill a 9200λ hole, but it is instructive to plot the radial distributions for this almost circular source model. Figure 4 shows the Fourier transforms of the MEM images, before convolving by a restoring beam. The radial distributions are plotted over the range of uv-spacings sampled by the 3 configurations, and map the model structure quite well except at the highest spatial frequencies which are not sampled uniformly in all directions. The break away from the input model occurs at the largest uv-distance sampled in all directions. The 3 lower curves show the difference images between the MEM images and the original model image, both convolved by the restoring beam. The image fidelity at different spatial frequencies is measured by the vertical distance from the model image. Configuration 1 samples a smaller range of uv-spacings than configurations 2 and 3. At declination +30, configuration 1 has a higher image fidelity, but at declination –30 this advantage is lost at the shortest spacings.

5. Conclusions

Configuration 1 is the most compact array and clearly gives the best brightness sensitivity for declinations up to $\sim$ +30 deg. Configurations 2 and 3 give comparable brightness sensitivity and sidelobes at higher declinations; Configuration 3 gives rounder beams above $\sim$ +30 deg, but configurations 2 is more versatile. Based on these results, it is hard to justify an extra $\sim$ \$1M to provide stations for configuration 3. Operationally, starting from configuration 1 observing unshadowed lower declination sources, one could alleviate the shadowing for high declination sources by selectively moving shadowed antennas into configuration 2 as one makes the transition into the intermediate configurations.

6. References

"Image Fidelity", M.C.H. Wright, 1999, BIMA memo 73, http://bima.astro.umd.edu/memo/memo.html

"Cross-talk in Close-packed Interferometer Arrays", Ravi Subrahmanyan, 2002, ATCA memo.

Table 1a: Beam FWHM and sidelobes levels excluding all shadowed data

Config	DEC	RMS[μJy]	Beam [arcsec]	Tb rms[μK]	Sidelobe[%]: RMS	Max	Min	Nvis[%]
config1	60	18.4	18.46 x 1.85	12	4.4	53.9	–56.7	2
config2	60	10.9	6.71 x 0.97	39	1.5	21.1	–17.2	5
config3	60	14.8	9.46 x 1.46	25	1.9	19.5	–12.3	3
config1	45	12.9	5.70 x 1.57	34	3.1	74.0	–33.7	4
config2	45	4.4	2.63 x 1.00	35	0.9	6.5	–4.4	32
config3	45	4.2	2.21 x 1.55	27	1.0	6.0	–4.5	35
config1	30	6.1	2.55 x 1.59	34	1.7	10.7	–5.1	17
config2	30	3.4	1.90 x 1.10	33	1.0	5.2	–3.1	55
config3	30	3.1	1.60 x 1.38	31	0.8	5.7	–4.9	63
config1	15	2.6	2.17 x 1.67	19	1.0	9.8	–4.5	93
config2	15	2.6	1.61 x 1.25	34	0.9	7.9	–1.9	93
config3	15	2.6	1.69 x 1.11	36	0.9	6.9	–4.4	95
config1	0	2.5	1.83 x 1.70	14	1.1	14.2	–4.7	100
config2	0	2.5	1.38 x 1.28	26	1.0	13.8	–2.8	100
config3	0	2.5	1.73 x 0.94	28	1.0	13.1	–4.4	99
config1	–30	2.5	1.70 x 1.69	16	0.9	8.8	–4.3	100
config2	–30	2.5	1.28 x 1.27	28	0.8	5.6	–1.7	100
config3	–30	2.5	1.74 x 0.87	30	0.8	4.8	–4.4	100
config1	–60	2.5	2.10 x 1.69	19	0.8	8.2	–4.6	96
config2	–60	2.5	1.58 x 1.26	34	0.7	4.9	–1.7	96
config3	–60	2.5	1.70 x 1.09	37	0.7	4.0	–4.5	97

Table 1b: Beam FWHM and sidelobes levels including data with up to 50% of antenna shadowed.

Config	DEC	RMS[μJy]	Beam [arcsec]	Tb rms[μK]	Sidelobe[%]: RMS	Max	Min	Nvis[%]
config1	60	7.6	10.50 x 1.73	10	1.2	10.5	–10.9	11
config2	60	4.2	6.92 x 1.14	11	0.7	8.5	–8.9	35
config3	60	4.2	6.09 x 1.66	9	0.7	5.3	–5.1	35
config1	45	2.7	4.36 x 1.68	10	0.6	7.1	–3.8	83
config2	45	2.6	3.28 x 1.27	17	0.6	4.4	–1.7	93
config3	45	2.6	2.30 x 1.68	18	0.6	3.1	–3.9	93
config1	30	2.5	2.82 x 1.70	10	0.9	8.5	–4.3	100
config2	30	2.5	2.11 x 1.28	17	0.8	5.5	–1.7	100
config3	30	2.5	1.70 x 1.44	18	0.7	3.4	–4.3	100
config1	15	2.5	2.14 x 1.70	12	0.9	9.1	–4.5	100
config2	15	2.5	1.61 x 1.28	22	0.9	7.4	–2.3	100
config3	15	2.5	1.71 x 1.10	24	0.8	6.2	–4.2	100

Table 2a: ALMA Single Field Imaging - CLEAN Deconvolution

Config	DEC	Beam[″]	scale[″]	Model Peak[Jy]	Total Flux	Peak	RMS
config1	–30	1.70 x 1.69	8	73.2	714	73.6	0.22
config2	–30	1.28 x 1.27	8	48.4	729	48.5	0.16
config3	–30	1.74 x 0.87	8	43.7	728	44.0	0.23
config1	30	2.82 x 1.70	8	110.1	721	110.1	1.19
config2	30	2.11 x 1.28	8	71.3	728	71.4	0.39
config3	30	1.70 x 1.44	8	64.4	728	64.3	0.27
config1	–30	1.70 x 1.69	16	26.5	408	23.5	0.09
config2	–30	1.28 x 1.27	16	17.2	322	14.8	0.13
config3	–30	1.74 x 0.87	16	16.1	290	13.7	0.15
config1	30	2.82 x 1.70	16	39.0	774	39.0	0.03
config2	30	2.11 x 1.28	16	25.2	733	24.8	0.06
config3	30	1.70 x 1.44	16	23.4	632	22.8	0.06

Table 2b: ALMA Single Field Imaging - MEM deconvolution

Config	DEC	Beam[″]	scale[″]	Model Peak[Jy]	Total Flux	Peak	RMS
config1	–30	1.70 x 1.69	16	26.5	731	26.6	0.035
config2	–30	1.28 x 1.27	16	17.2	731	17.2	0.024
config3	–30	1.74 x 0.87	16	16.1	731	16.1	0.040
config1	30	2.82 x 1.70	16	39.1	731	39.1	0.072
config2	30	2.11 x 1.28	16	25.2	731	25.2	0.021
config3	30	1.70 x 1.44	16	23.4	731	23.3	0.032
config1	–30	1.70 x 1.69	24	14.2	681	13.8	0.098
config2	–30	1.28 x 1.27	24	8.9	704	8.8	0.031
config3	–30	1.74 x 0.87	24	8.4	710	8.3	0.028
config1	30	2.82 x 1.70	24	21.0	731	20.9	0.025
config2	30	2.11 x 1.28	24	13.2	731	13.3	0.022
config3	30	1.70 x 1.44	24	12.5	731	12.4	0.017
config1	–30	1.70 x 1.69	32	8.9	632	8.3	0.32
config2	–30	1.28 x 1.27	32	5.4	612	5.2	0.15
config3	–30	1.74 x 0.87	32	5.4	594	4.9	0.14
config1	30	2.82 x 1.70	32	13.3	717	13.1	0.03
config2	30	2.11 x 1.28	32	8.2	724	8.2	0.02
config3	30	1.70 x 1.44	32	7.8	720	7.7	0.02

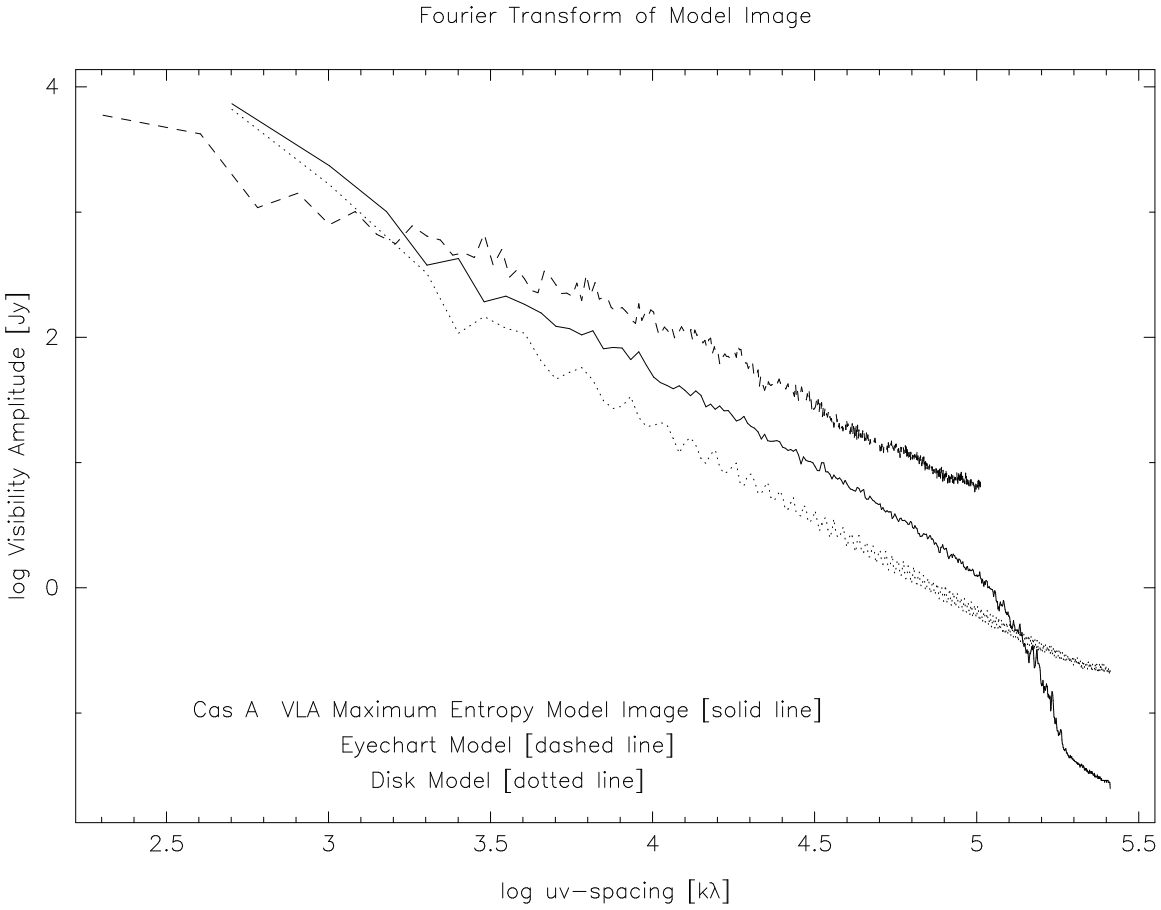

Fig. 1.— Radial distribution for Fourier Transform of 3 source models

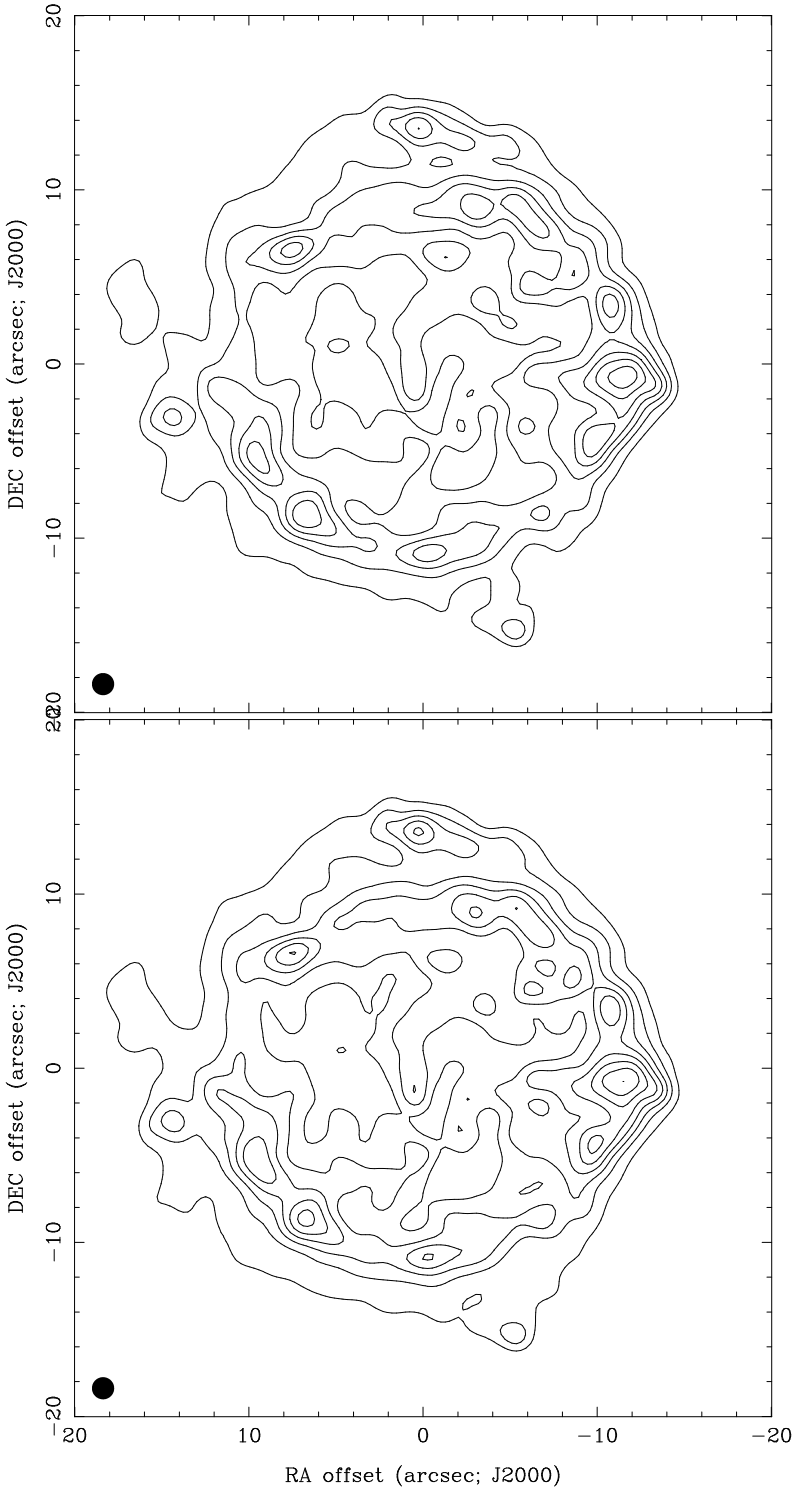

Fig. 2.— Maximum Entropy Image [upper panel] and Cas A model [lower panel] 1/10 full scale, imaged with ALMA compact configuration 2 at declination –30 deg. Contours at 12.5 %

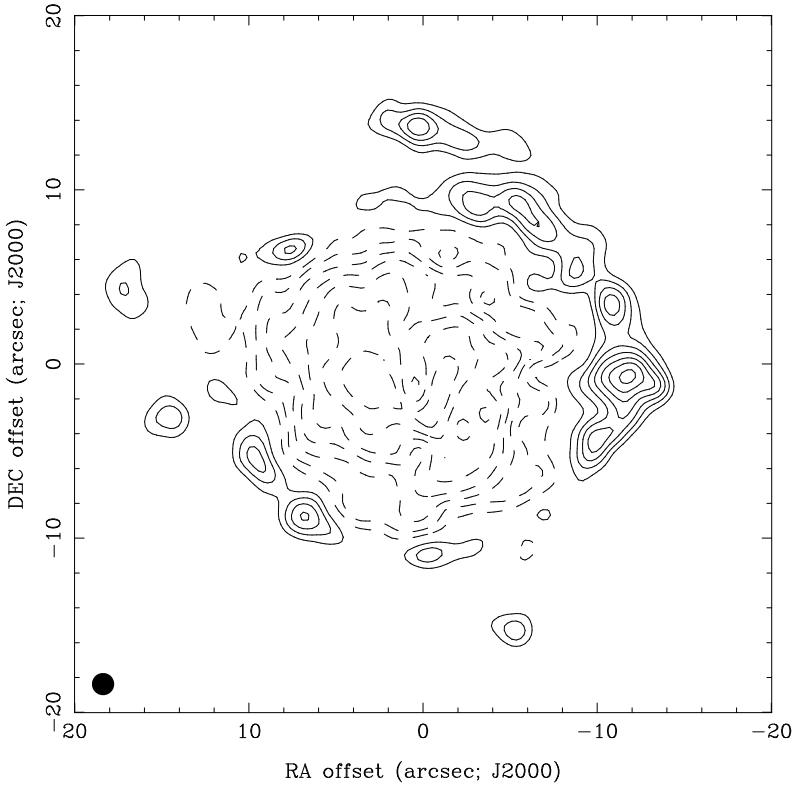

Fig. 3.— Residual Image for configuration 2 at declination –30 deg. Contours at 1.4 % of Maximum Entropy Image.

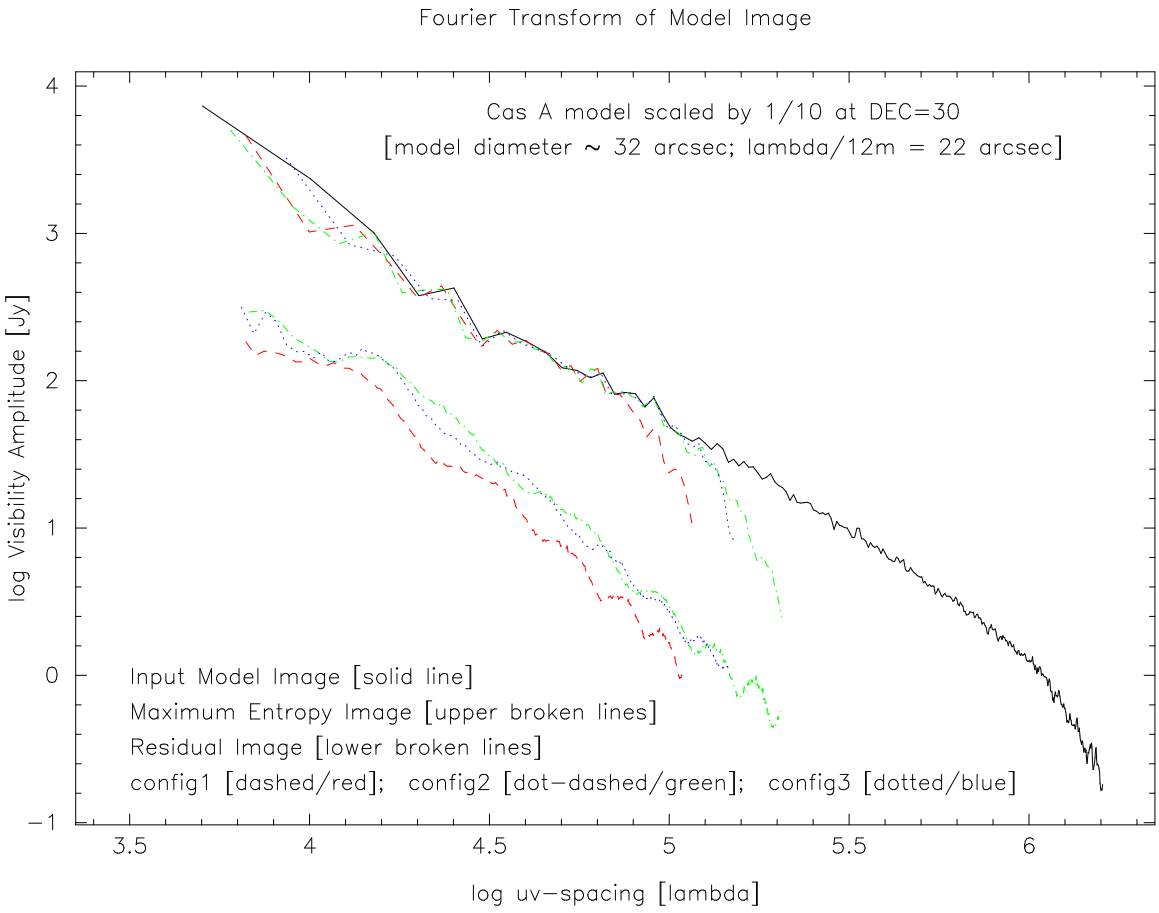

Fig. 4.— Radial distribution for Fourier Transform of Cas A model scaled by 1/10 at DEC=30

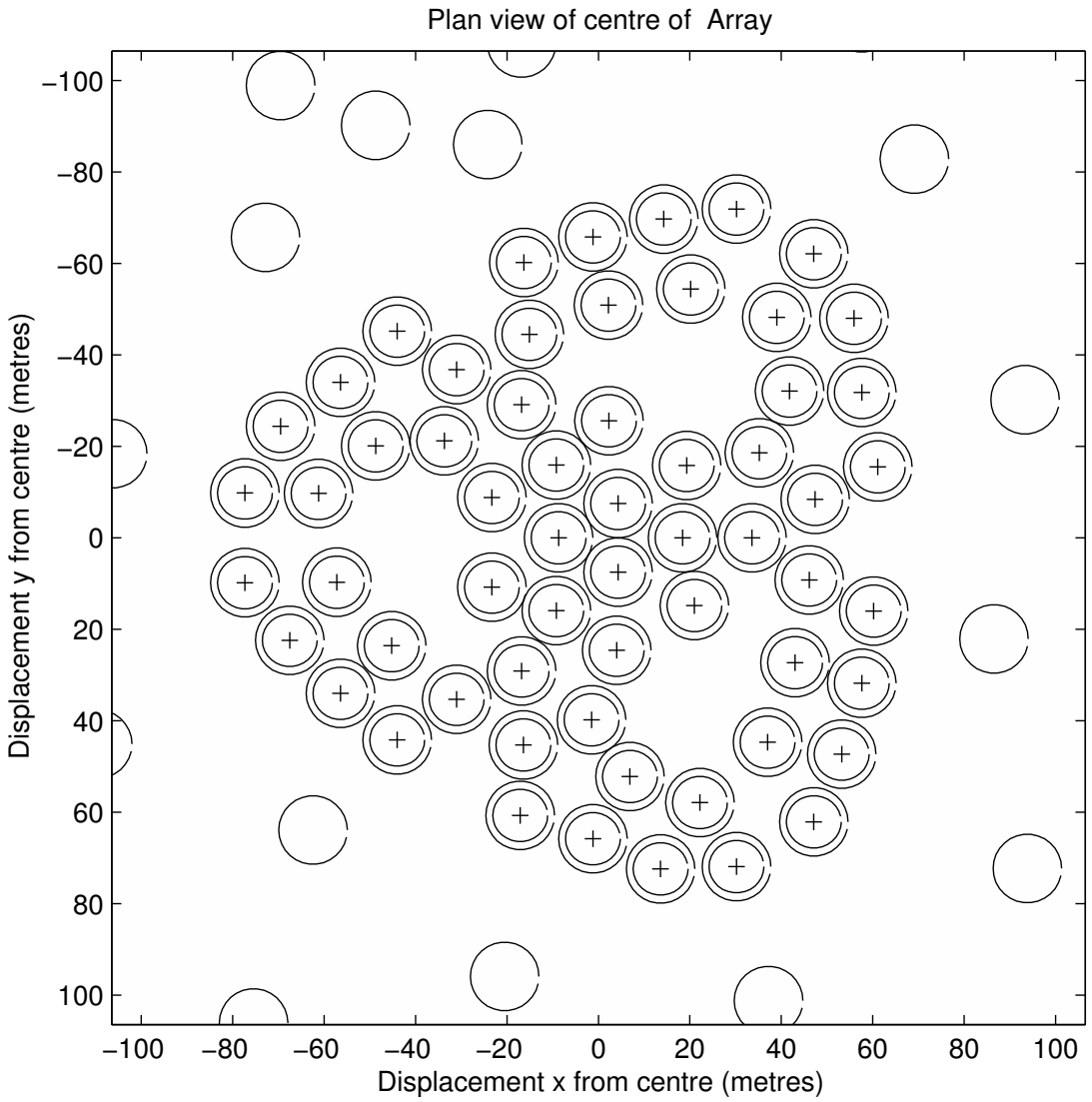

Fig. 5.— Config 1 - A most compact array for maximum brightness sensitivity. The inner circles are the 12m diameter antennas. The outer circles are 15m diameter, and indicate the collision diameter and the unoccupied pads (J.Conway private communication).

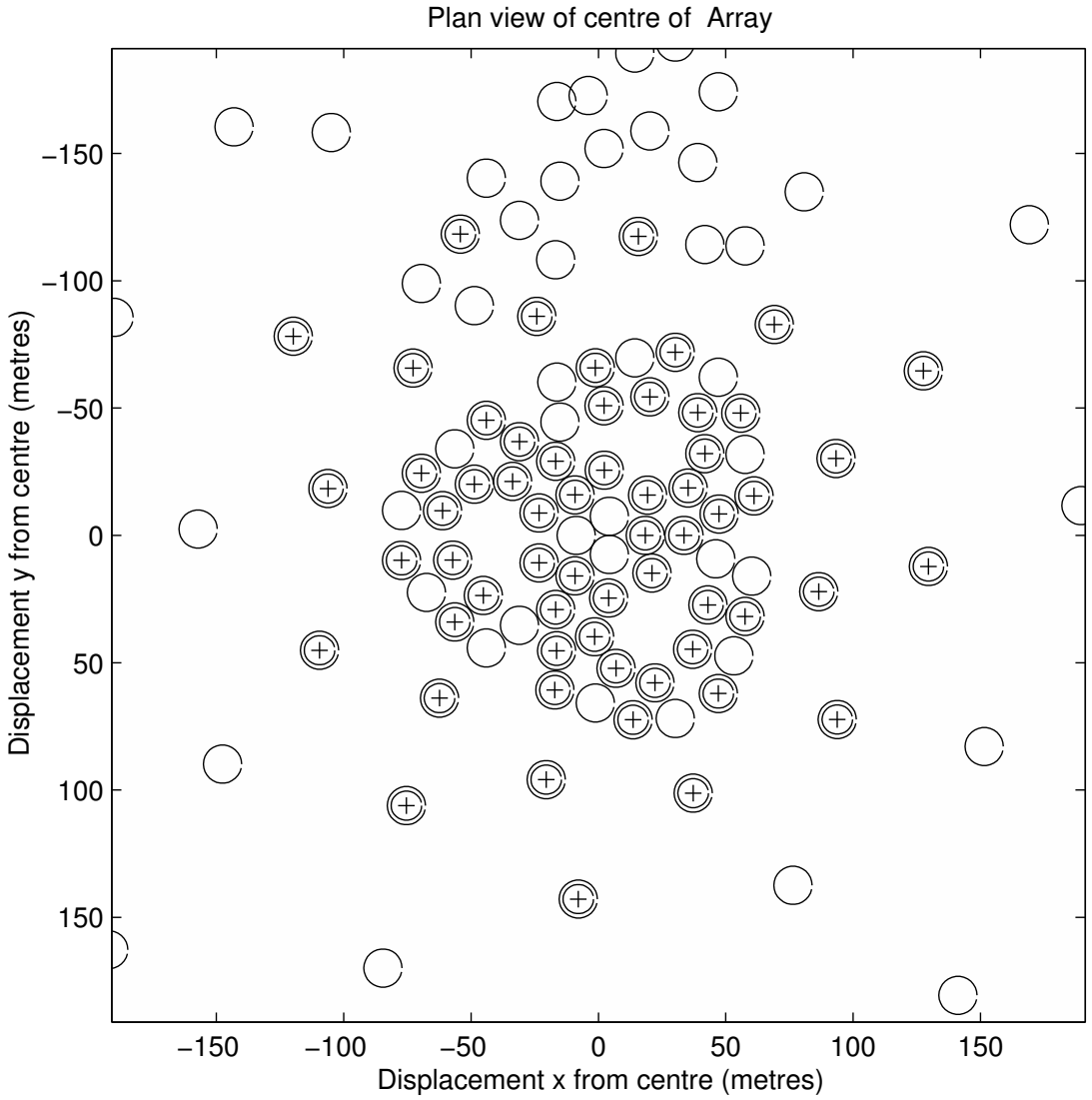

Fig. 6.— Config 2 - A more Gaussian array with 1.5 times the resolution of config 1.

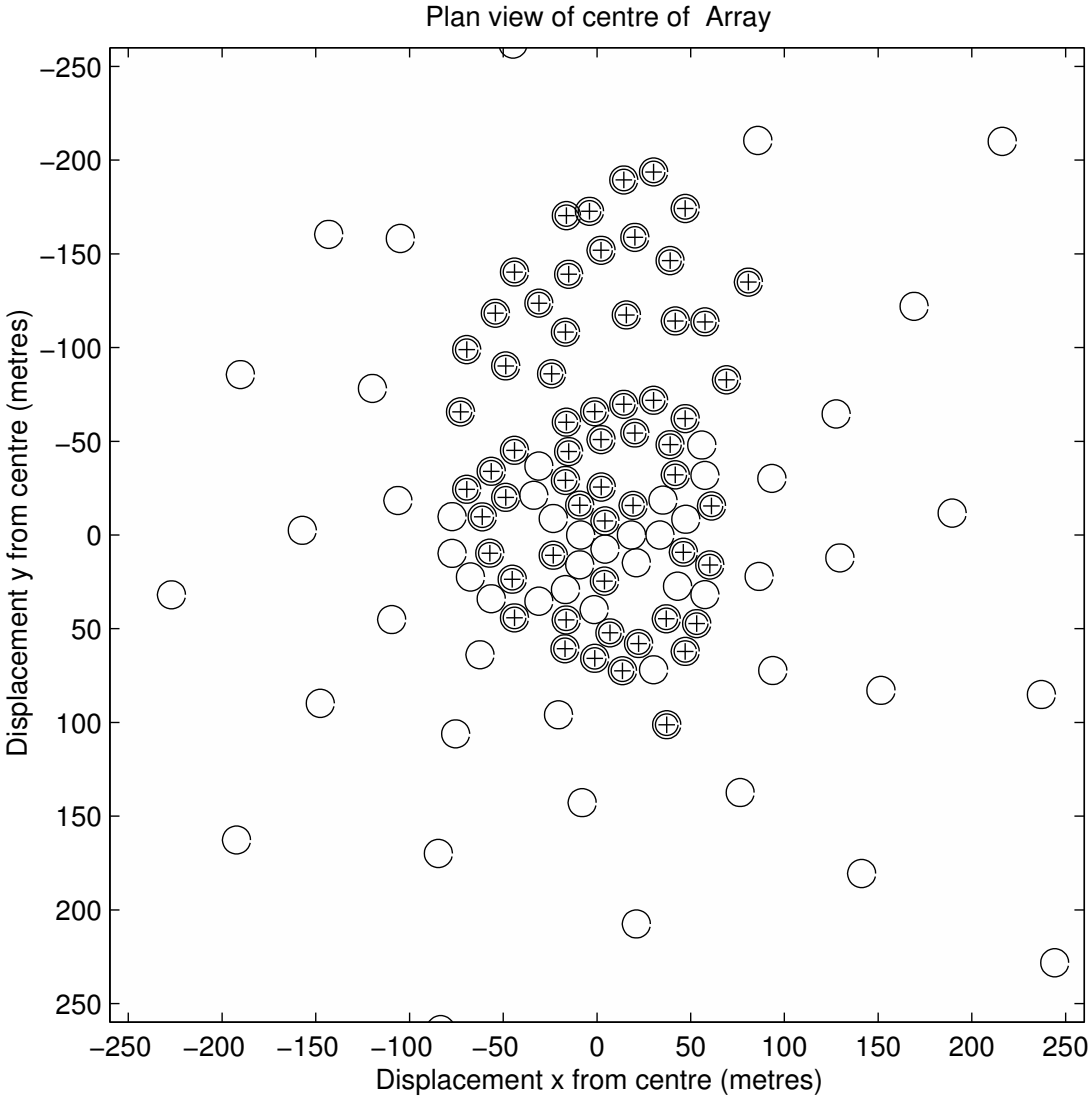

Fig. 7.— Config 3 - A N-S extended array with a circular beam and the same resolution as config 1 for declination 30 deg sources.